Neutron Scattering Study on Spin-Peierls Transition in $CuGeO_3$

$CuGeO_3$ における
スピン・パイエルス転移の
中性子散乱による研究

西　正和

①

Thesis

Neutron Scattering Study on
Spin-Peierls Transition in $CuGeO_3$

$CuGeO_3$ におけるスピン・パイエルス
転移の中性子散乱による研究

Masakazu   Nishi

西　　正和

The Institute for Solid State Physics,

University of Tokyo

東京大学　　物性研究所

December, 1994

Acknowledgments

Abstract

Magnetic excitations in the novel inorganic spin-Peierls (SP) system $CuGeO_3$ have been studied by means of inelastic neutron scattering. The formation of a gap state due to the structural dimerization in the Cu-O_2-Cu chain along the c-axis with a gap energy of about $\Delta_{sp} = 2$ meV was observed at T_{sp} (= 14 K) for the first time in a SP system. In the dimerized state ($T < T_{sp}$) the character of the excited state was determined by investigating the magnetic field dependence of the gap state. An application of the magnetic field in three different directions demonstrates the isotropic and triplet nature of the gap state. Polarized neutron inelastic scattering directly evidences the triplet states for the spin fluctuation components of these Zeeman split under an applied field. All these results strongly underline the excitonic description of the singlet-triplet transition in this alternating antiferromagnetic (AF), $S=1/2$ chain system. Detailed study of spin excitation dispersion relations in the dimerized state shows that $CuGeO_3$ below T_{sp} can be regarded as weakly coupled alternating, $S=1/2$ AF chain system. The intra-chain and inter chain exchange parameters were determined as $J_c \approx 10.4$ meV, $J_b \approx 0.1\ J_c$, and $J_a \approx -0.01\ J_c$ by the Heisenberg AF spin wave formula. Line shape analysis shows a pronounced asymmetry, suggesting the existence of a spin wave double continuum similar to the case of a uniform $S=1/2$ AF chain.

Under hydrostatic pressure up to 1.8 GPa, the SP gap, Δ_{sp} increases linearly with increasing pressure. This fact is consistent with the increase of T_{sp} under pressure observed by Takahashi *et al.* However, intra-chain exchange interaction, J_c decreases with increasing pressure.

In addition to these extensive magnetic excitation measurements,

lattice dynamics in this SP system have been also studied by inelastic neutron scattering. No appreciable softening of any phonon branch was observed. An anomalous broad phonon line width was observed for the [001] longitudinal phonon at about 21 meV near the Brillouin zone boundary. However, the phonon profile did not change around T_{sp}.

From the magnetic critical scattering, the magnetic correlation length did not agree with the calculated value by using the anisotropic magnetic exchange constants in a usual antiferromagnetic order.

Contents :

Chapter 1.   Introduction

Low-dimensional magnetic systems, especially quantum spin systems, have attracted much attention during recent years both theoretically and experimentally. The theoretical interest has been focused on the $S=1/2$ linear Heisenberg antiferromagnetism (AF) since Bethe's exact solution for its ground state [1]. Its spin dynamics was theoretically investigated by des Cloizeaux and Pearson [2] who revealed a dispersion relation for excited states, being very similar to the semi-classical Anderson's spin wave results with renormalized zone boundary energy. Endoh *et al.* performed the first inelastic neutron scattering experiment on $CuCl_2 \cdot 2N(C_5D_5)$, dichloro *bis* pyridine copper II (CPC) [3], and experimentally evidenced the des Cloizeaux and Pearson's dispersion results. They also observed an asymmetry in the line shape of the spin excitation spectra. Subsequently, the exact calculation using finite chain showed the existence of the spin wave double continuum (SWDC), which could explain their neutron scattering results. The dispersion relation by des Cloizeaux and Pearson turned out to be the lower boundary of this SWDC. More recently, the existence of the SWDC was confirmed in $KCuF_3$ by an inelastic neutron scattering using a chopper time of flight spectrometer at the spallation source [4].

In 1983 Haldane proposed that the spin dynamics depends on the spin value, whether being half-integer or integer. In particular, he pointed out that $S=1$ AF Heisenberg chain should have an energy gap for excited triplet state even at the zone center [5]. This Haldane gap initiated both theoretical and experimental controversies, because it was contradictory to the expectation of the semi-classical spin wave theory discussed so far. After many intensive studies both theoretically and experimentally this controversy has been settled in

1

favor of Haldane's idea.

The $S=1/2$ linear alternating Heisenberg chain has also been a long standing theoretical and experimental problem. It has attracted theoretical and experimental attention for about two decades, particularly in relation to the spin exciton theory and the properties of linear exchange coupled free radicals. Static properties like magnetic susceptibility were calculated for this system and compared with the experimental results on free radical solid. Spin dynamics in these systems have also been discussed theoretically pointing to a possible Wannier state for a small alternation parameter. More recently, with the discovery of spin-Peierls (SP) system this alternating Heisenberg chain became of increasing interests for physicists.

The SP transition must be accompanied with an intrinsic lattice instability in a system of quantum mechanical AF chains where the spins are interacting via a Heisenberg or XY exchange interaction and the chains are coupled to a three dimensional phonon. At the critical temperature, called SP temperature T_{sp}, a second order transition occurs and a dimerized state is stabilized below T_{sp} where a system can be regarded as an ideal linear alternating AF.

Experimentally the SP transition was first observed in the organic compound TTF-CuBDT [6] by magnetic susceptibility and EPR measurements. Subsequently, several other organic compounds such as MEM-$(TCNQ)_2$ [7], TTF-AuBDT [8], and SBTTF-TCNQCl$_2$ [9] were reported [7,10]. In all these organic SP systems the evidence for the SP transition was obtained either by observation of the dimerization in the lattice or by the macroscopic magnetic measurements of magnetization or susceptibility. Because of the limited crystal size available for the organic SP substances, however, direct observation of spin dynamics using neutron scattering has not

2

been possible.

Recently Hase *et al.* (1993) [11] reported the existence of the SP transition in an inorganic $CuGeO_3$. Their single crystal measurement clearly indicated that its magnetic susceptibilities rapidly drop to zero along three principal axes below the SP transition temperature T_{sp} (= 14 K) as shown in Fig. 1. The peak position of Bonner-Fisher [12] curve is adjusted to the maximum value of the magnetic susceptibility, but it cannot fit well to the observed value in contrast to that of TTF-CuBDT [6]. They also observed the magnetic field dependence of the phase transition temperature $T_{sp}(H)$ of polycrystalline $CuGeO_3$, and demonstrated that its magnetic phase diagram is in qualitative agreement with that of an organic SP system [13]. The SP transition temperatures T_{sp} and AF exchange interactions J of $CuGeO_3$ [14] and organic SP substances [6,7,8,9] discovered so far are shown in Table 1 with the spin lattice coupling constants η', SP gaps $\Delta(0)$ at $T = 0$ K, and $2\Delta(0) / k_B T_{sp}$. T_{sp} and J of $CuGeO_3$ show the intermediate values among these substances. The comparison of these basic parameters implies that the SP transition mechanism of $CuGeO_3$ are basically the same as those of other organic compounds.

This particular transition doesn't occur in the majority of quasi-one-dimensional AF inorganic compounds because of the necessary conditions as follows [8] ; (1) a one-dimensional material is most suitable, (2) the material must be an insulator, not a metal, (3) a spin quantum number of 1/2 is required, (4) an AF intra-chain exchange constant is necessary and (5) the intra-chain exchange interaction must not be of the Ising type.

The spin system requires a magnetically singlet ground state with an energy gap accompanied with the lattice dimerization. If the dimerization occurs, the unit cell doubles along the chain direction

3
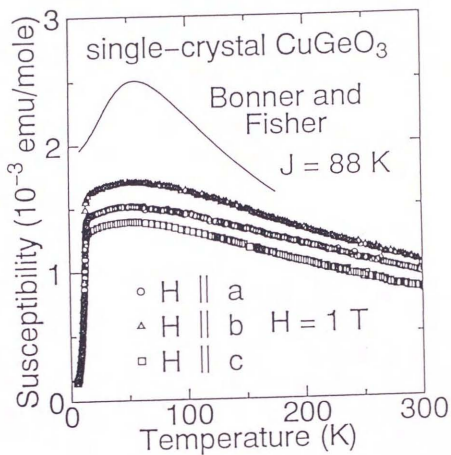
Fig.1. Magnetic susceptibility on $CuGeO_3$ along three principal axes by Hase *et al.* [11].   Bonner-Fisher curve was adjusted at the maximum value of magnetic susceptibility.

Table1. Spin-Peierls compounds with the transition temperature T_{sp}, the intra-chain exchange interactions J, spin-lattice coupling constants η', spin-Peierls gaps $\Delta(0)$ at $T=0$ K and $2\Delta(0) / k_B T_{sp}$, where J is defined by following Hamiltonian:

$$H = J \sum_i S_i \cdot S_{i+1} \text{ and } \eta' \text{ is equal to } T_{sp} / 0.8\, J$$

	T_{sp}	J/k_B	$\eta' = T_{sp}/0.8J$	$\Delta(0)$ (K)	$2\Delta(0)/k_B T_{sp}$
CuGeO$_3$ [11,14]	14	121	0.145	24.5	3.50
TTF-CuBDT [6]	12	77	0.195	21	3.50
TTF-AuBDT [8]	2	68	0.037	3.7	3.70
MEM-(TCNQ)$_2$ [7]	18	106	0.209	56	3.11
SBTTF-TCNQCl$_2$ [9]	38	160	0.297	67	3.52

and a new satellite peak should appear at $\ell = 0.5$. Recently, electron [15] and x-ray diffractions [16] independently confirmed the presence of superlattice reflections at $(h+1/2, k, \ell+1/2)$ with h, ℓ integers and k odd number. The subsequent neutron scattering study [17] evidenced the dimerization of the Cu atoms along the c-axis, confirming that $CuGeO_3$ is a typical SP system. The out-of-phase dimerization of the neighboring chains along the a or b-axis indicates a finite inter chain interaction. In the neutron scattering experiment, the superlattice reflections with k even number were also observed as a result of the shift of the O atom positions in the a-b plane [17]. A spontaneous contraction strain below T_{sp} along the b-axis was also observed by neutron [18] and x-ray [19] diffractions. Anomalies in the lattice dynamics, most probably associated to this strain, have been studied by inelastic neutron scattering [18].

Since a large single crystal of $CuGeO_3$ (typically $45 \times 10 \times 3$ mm^3 in size) has been available, detailed study of the spin dynamics by means of inelastic neutron scattering in a SP system has been possible.

We thus performed inelastic scattering experiments using both unpolarized and polarized neutrons to study spin dynamics in dimerized ($T < T_{sp}$) and normal ($T > T_{sp}$) state in $CuGeO_3$. Since the SP transition is related to the lattice instability, a lattice dynamical study was also performed.

6

Chapter 2.   Experimental

2-1. Crystal Structure

The crystal structure of $CuGeO_3$ is orthorhombic ($\mathbf{D}_{2h}^5 - \mathbf{P}_{bmm}$) with $a = 4.81$ Å, $b = 8.47$ Å, and $c = 2.94$ Å at room temperature [20]. This structure is built up by $[CuO_2]^{2-}$ and $[GeO_3]^{2-}$ linear chains along the c-axis in which a copper atom is located at the center of the square of four oxygen atoms with the short Cu-O distances (1.94 Å) as shown in Fig. 2. The superexchange interactions between the Cu^{2+} spins at $z = 0$ and 1 are mediated by two shortest bound oxygens located at $z = 1/2$. Hence it is expected that these $Cu-O_2$-Cu bonds form quasi-one-dimensional AF chains along the c-axis.

7
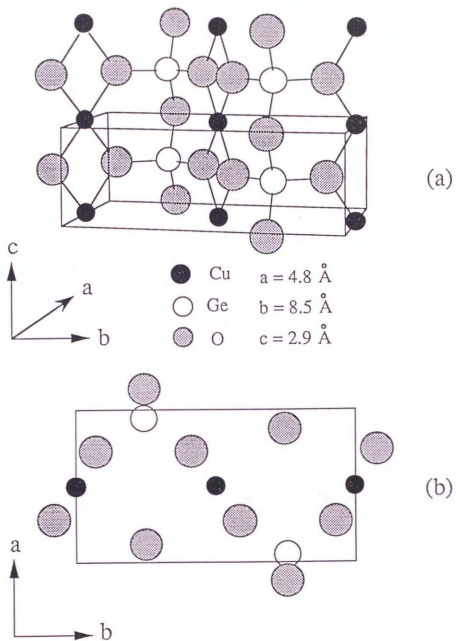
Fig. 2. Crystal structure of $CuGeO_3$. CuO_2 and GeO_3 linear chains are along c-axis.

2-2. Sample Preparation

Powders of CuO (99.99 % Rare Metallic CO., LTD.) and GeO_2 (99.999 % Furuuchi Chemical CO., LTD.) were mixed stoichiometrically and the water contained in the mixture was removed in vacuum for about 12 hours at 250 °C. This sample was transacted to a quartz tube which was evacuated and placed in the furnace heated to 1100 °C and kept for 48 hours. Then the furnace was cooled gradually to room temperature. Many needle like single crystals grew up in the turquoise blue powder. This powder sample used for the neutron powder scattering [21] was confirmed not to contain impurities by x-ray scattering. $CuGeO_3$ single crystals were kindly supplied by O. Fujita and J. Akimitsu at Aoyama Gakuin University. Their growing procedures are described in the following. The powder sample was pressed into a rod (7 mmØ×100 mm) and sintered at about 1000 °C. A single crystal was grown by a traveling floating zone method. Growth rate in a floating zone process was 1 mm per hour under O_2 gas flowing. The single crystal obtained was transparent blue with the size of $45×10×3$ mm^3 and a plate-like shape. X-ray diffraction and magnetization measurements confirmed that it was a single-phased $CuGeO_3$. Magnetization measurements showed that data were in good agreement with that of Hase *et al.* [11], such that the magnetization drastically dropped to zero at 14 K along three principal axes.

2-3. Neutron Scattering

Neutron scattering experiments were performed on the POlarized Neutron Triple Axis (ISSP-PONTA) and High Q Resolution (ISSP-HQR) spectrometers installed at JRR-3M reactor at Japan Atomic Energy Research Institute (JAERI), Tokai, Japan. The (0 0 2) reflection of pyrolytic graphite (PG) was used for both monochromator and analyzer, and a PG filter was placed behind the sample to eliminate higher order contamination. The typical experimental condition at PONTA was as follows; the incident energy of neutron E_i=14.77 meV, the wave length $\lambda = 2.353$ Å and the collimation open(40')-40'-40'-40'. When PG filters were set both before the monochromator and between the sample and the analyzer, the half λ intensity was an order of 10^{-6}. In HQR spectrometer, we used the double axis mode with the incident neutron energy E_i=13.84 meV, the wave length $\lambda = 2.431$ Å and the collimation open(6')-open (30')-40'. When the PG filter was set between the monochromator and the sample, the half λ contamination became below 10^{-3}.

Chapter 3. Magnetic Excitations

3-1. Temperature dependence

(1) $T < T_{sp}$

We performed the first inelastic neutron scattering to study the magnetic excitations in $CuGeO_3$[14]. For the quasi-one-dimensional SP system, the excitation dispersion spectrum is generally known to have an energy gap at $q = 0$. In addition, this alternating spin singlet state changes to a uniform state above T_{sp} and the finite energy gap vanishes at the center of Brillouin zone. The sample was mounted in an Al can filled with helium gas and attached to the cold head of a closed cycle helium refrigerator which could cool to 4 K. Crystal axis was set with the [100] direction vertical in the b^*-c^* scattering plane. To observe such phenomena, we measured the temperature dependence of the neutron scattering intensity at an energy transfer $\Delta E = 1$ meV at the lower energy of the SP gap ($q = 0$) using the triple axis mode with $E_i = 13.7$ meV at (0, 1, 0.5). As shown in Fig. 3, the neutron scattering intensity increases with decreasing temperature, reaches its maximum at about $T_{sp} = 14$ K, and then exponentially decreases below T_{sp} due to the formation of the SP gap. An overdamped mode occurs in the intensity profile above T_{sp}, therefore, the intensity gradually decreases as temperature is increased. It should be noted that the excitation spectrum from the singlet ground state to the excited triplet state should occur below T_{sp}, although the resultant excitation peaks around $T = 14$ K are not spin waves in a strict sense, since no long-range magnetic order exists. Thus, these propagating quasiparticles in the excited triplet state should be called "magnetic excitons" instead of magnons. The temperature dependence of the magnetic exciton profiles of $CuGeO_3$ at (0, 1, 0.52) is shown in Fig. 4 for $E_i = 13.7$ meV and collimator

11
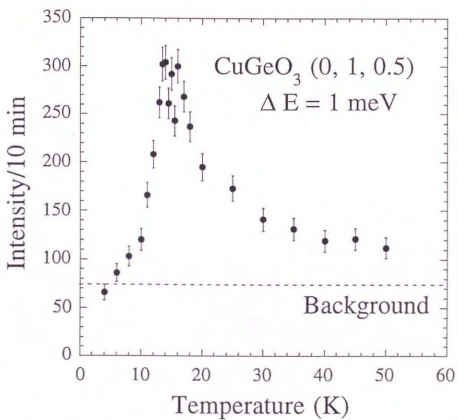
Fig. 3. The temperature dependence of the neutron scattering intensity at $\Delta E = 1$ meV at $q = 0$.
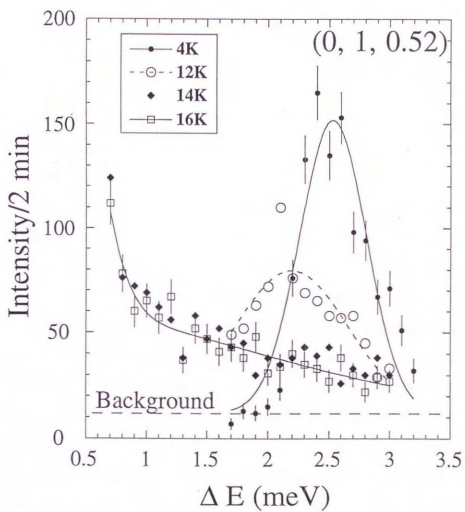
Fig. 4. Energy scan profiles of the magnetic exciton at (0, 1, 0.52) for various temperatures with $E_i = 13.7$ meV.

setting; open(40') -40'-40'-80', where a very sharp peak is seen at 4 K. The magnetic exciton at $q = 0.02\ c^*$ has a wavelength 50 times larger than that of the lattice constant c. Note that at 12 K the peak becomes broader and weaker and shifts to lower energy, while at 14 K the SP energy gap completely vanishes and the magnetic excitations are simultaneously overdamped. The neutron scattering profiles between 14 and 16 K are very similar and show a FWHM of about 4 meV around $\Delta E = 0$ meV.

Figure 5 shows the dispersion relations of the magnetic excitons along each principal axis ($a,\ b,$ and c), where it is obvious from these results that $(0, 1, 0.5)$ is the zone center. Since the strongest correlation energy occurs along the c^*-axis parallel to the direction of the CuO_2 chain, this confirms that $CuGeO_3$ has a one-dimensional magnetic character along this axis. Using the des Cloizeaux and Pearson formula [2], the characteristic energy for a one-dimensional excitation is $\pi J_c /2 = 16.3$ meV. However, the intra-chain exchange parameter $J_c = 10.4$ meV (120.4 K) is larger than the expected value $J_c = 7.58$ meV (88 K) obtained from magnetic susceptibility data [11]. Other zone boundary (ZB) energies were obtained as E_b^{ZB}=5.6 meV at $(0, 0, 1/2)$ and E_a^{ZB}=2.7 meV at $(1/2, 1, 1/2)$, which is the superlattice point [15, 16, 17] in the dimerized crystal structure. It should be noted that the magnetic zone center is different from the structural superlattice point. To estimate the inter chain exchange constants, we analyzed our data in terms of the Heisenberg antiferromagnetic Hamiltonian $H = \sum_{ij} J_{ij} \hat{S}_i \hat{S}_j$. The dispersion relation can be obtained from the Heisenberg antiferromagnetic spin wave formula [22], i.e.,

$$\left\{ E(q) \right\}^2 = \left\{ (\pi/2)J_c + J_b + E_A - J_a(1 - \cos 2\pi h) \right\}^2$$

14
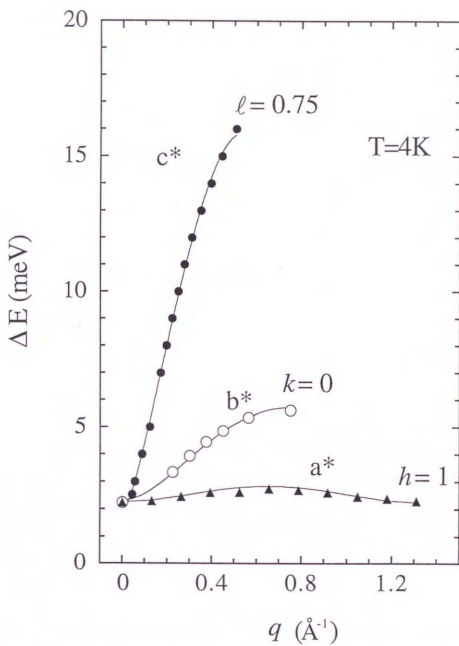
Fig. 5. The dispersion relations of the magnetic excitons in CuGeO$_3$ along each principal axis at $T = 4$ K. The solid lines indicate resultant curve fittings using the Heisenberg antiferromagnetic spin wave formula. (0, 1, 1/2) is the zone center; $q = 0$.

$$-\left\{(\pi/2)J_c \cos 2\pi\ell + J_b \cos \pi k\right\}^2, \qquad (1)$$

where J_a, J_b, and J_c are, respectively, the exchange parameters along each principal axis and the uniaxial anisotropic magnetic energy E_A is used to replace the SP energy gap. Consequently, the exchange energies along the b- (J_b) and a-axes (J_a) were, respectively, estimated as $J_b \approx 0.1\ J_c$ and $J_a \approx -0.01\ J_c$.†

The one-dimensionality of $CuGeO_3$ is not so pronounced as $KCuF_3$, being a quasi-one-dimensional quantum AF system [24].

The temperature variation of the SP energy gap at (0, 1, 0.5) is shown in Fig. 6, where the gap energy is 2.1 meV at 0 K. Using this energy, a value of ß ≈ 0.093 was determined by

$$\Delta(T) = \Delta(0)\ (1 - T/T_{sp})^\text{ß}, \qquad (2)$$

where $T_{sp} = 14$ K.

For the one-dimensional Heisenberg spin system with $S = 1/2$, quantum mechanical dispersion relation formula was proposed by des Cloizeaux and Pearson, as

$$E = \pi J_c/2\ |\sin(2\pi\ell)|. \qquad (3)$$

The dynamical spin-correlation function in (q,ω) space was calculated by Müller et al. [25]. They showed that eq. (3) only gives the lower energy boundary of a magnetic excitation continuum which is called

---

† After submitting this thesis, we received the paper from Katoh and Imada [23]. They derived the dispersion formula of SP system including the inter chain exchange constant. The fitting procedure to our data for their theoretical formula is now in progress.

16
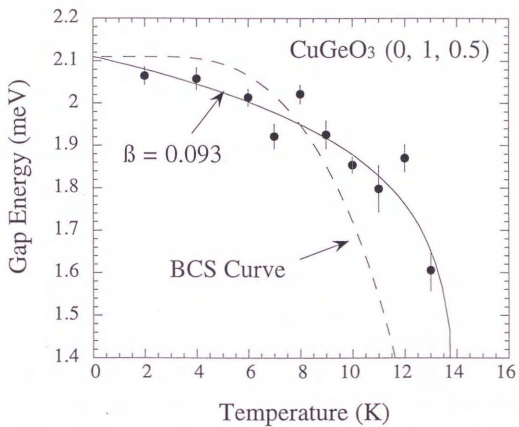
Fig. 6. The temperature dependence of the spin-Peierls gap at the zone center (0, 1, 0.5). Calculated results using eq. (2) and BCS curve are also shown.

spin-wave double continuum (SWDC). The upper boundary of SWDC was given by Bonner and Blöte [26] as

$$E = \pi J_c \ |\sin(\pi\ell)\ | .\qquad\qquad(4)$$

SWDC as an expression of quantum effects in an AF Heisenberg linear chain was observed as asymmetric line shapes in neutron scattering experiments on CPC [3] and $KCuF_3$ [24]. Recently, Nagler et al. [4] confirmed SWDC up to upper boundary in $KCuF_3$ with pulsed neutron source. In our measurements on $CuGeO_3$, asymmetric line shapes are observed in Figs. 7 (a) and (b), where the deviations from the Gaussian line shape on the high energy side may be attributed to SWDC. In the constant energy scan in Fig. 8, similar discrepancies to Gaussian fitting curve were also seen at low q side which cannot be accounted for by the resolution effects. These additional intensities should be therefore attributed to SWDC. Hence, these results clearly demonstrate the existence of SWDC above the lowest excitation boundary in the dimerized $S = 1/2$ spin chain. The one dimensionality is maintained even at low temperature in spite of the rather large inter chain exchange ($J_b /J_c \sim 1/10$), because the correlation lengths in the individual chain do not diverge but remain finite due to the singlet nature of the dimerized $S = 1/2$ chain.
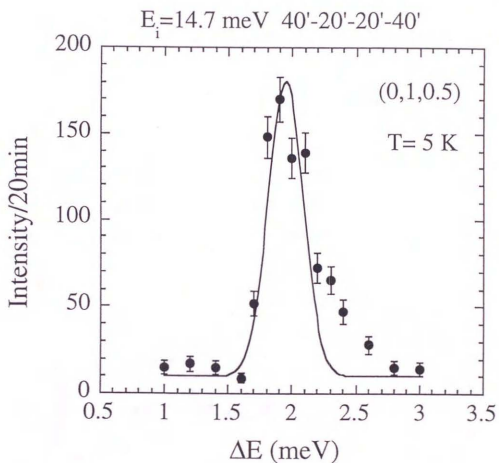
Fig. 7. (a) Magnetic excitation at magnetic zone center, (0,1,0.5) with fixed incident neutron energy, $E_i = 14.7$ meV and collimations, 40'-20'-20'-40' at $T = 5$ K. Solid line is a Gaussian fitting curve to the data except for the four deviating points on the high energy side.
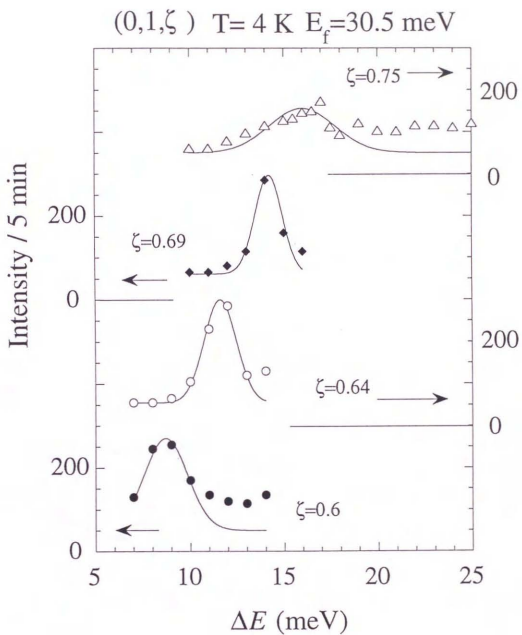
Fig. 7. (b) The magnetic excitation profiles at several q with fixed final neutron energy, E_f = 30.5 meV and collimations, open(40')-40'-40'-80' at 4.2 K.

20
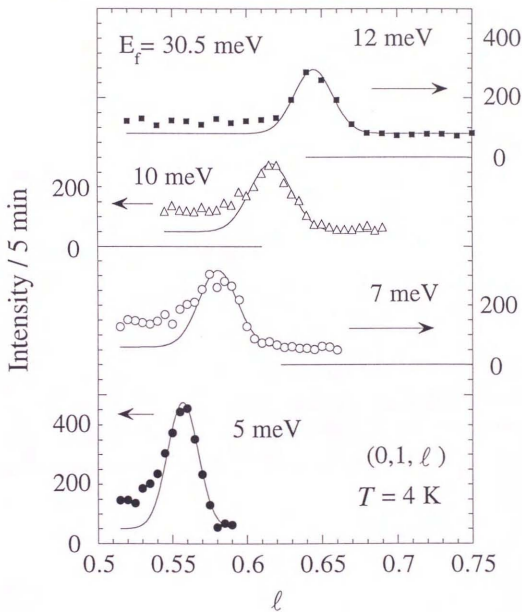
Fig. 8. Magnetic excitation profiles in constant energy scan with fixed final neutron energy, E_f = 30.5 meV at 4.3 K.

(2) $T > T_{sp}$

As shown in Fig. 5 $CuGeO_3$ has a one-dimensional magnetic character along the c^*-axis parallel to the direction of the CuO_2 chain [14].

Above T_{sp} the alternating spin singlet state changes to a uniform state and the finite energy gap vanishes at the Brillouin zone center. To observe the critical scattering above T_{sp}, the temperature dependence of the neutron scattering intensity was measured around (0, 1, 1/2) using the double axis configuration with incident neutron energy E_i=30.5 meV and collimation open(40')-20'-20' [27]. As shown in Fig. 9, one can see that with decreasing temperature, the neutron scattering intensity at (0,1.05,0.5) increases critically, reaches its maximum at T_{sp}, and then exponentially decreases below T_{sp} due to the formation of the singlet pair ordering.

We measured the neutron scattering intensity by the step scans parallel to c^*- and b^*-axes through (0, 1, 1/2) at 15.3 K. The neutron scattering cross section in the quasi-elastic approximation is proportional to the wave vector dependent susceptibility, $\chi(q)$. $\chi(q)$ is represented by the Lorentzian spatial distribution in the Marshall and Lowde's formalism [28] as follows:

$$\chi(0,q_b,0) = \frac{B}{\xi_b^{-2} + q_b^2} \qquad (5)$$

and

$$\chi(0,0,q_c) = \frac{C}{\xi_c^{-2} + q_c^2} , \qquad (6)$$

where B and C are constants and

$$\frac{\xi_c}{\xi_b} = \frac{c^2}{(b/2)^2} \frac{J_c}{J_b} . \qquad (7)$$

22
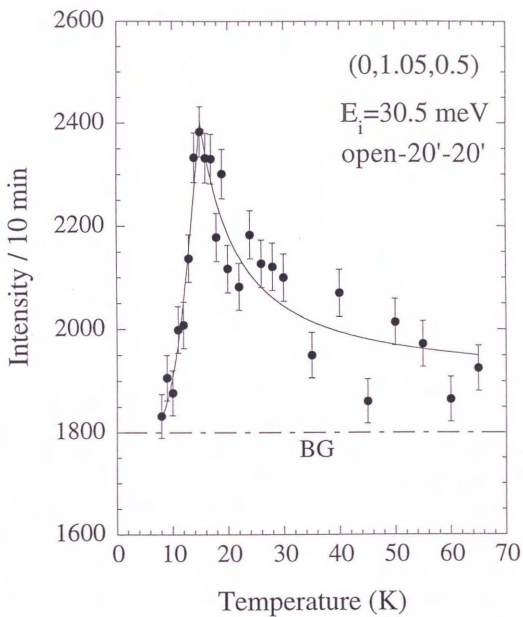
Fig. 9. The temperature dependence of the critical scattering intensity with double axis mode at (0,1.05,0.5).   Lines are guides to the eye.

We obtained experimentally the correlation lengths as $\xi_c=12\pm1$ Å and $\xi_b=4.1\pm0.3$ Å from eqs. (5) and (6) as shown in Fig. 10. Using the exchange constants, J_b and J_c obtained from the dispersion relation, the ratio ξ_c/ξ_b is estimated to be 12 from eq. (7). However, the observed ratio ξ_c/ξ_b =2.9±0.4 at 15.3 K is not in agreement with the calculated value but in agreement with the ratio of structural correlation lengths, 3.1 previously obtained by Pouget *et al.* [16] from the structural fluctuations measured by x-ray scattering.

Figure 11 shows the magnetic excitation spectrum at $(0, \bar{1}, 0.65)$ measured with fixed incident neutron energy E_i=30.5 meV and the open(40')-40'-40'-80' collimation at different temperatures. Although the peak intensity decreases with increasing temperature, an underdamped excitation at 29 K is still visible at the same energy as at 8 K. Since the magnetic excitation at $Q=(0, \bar{1}, 0.6)$ is already damped at this temperature, one can estimate the magnetic correlation length ξ_c to be ~7 Å at 29 K from the empirical formula λ_c~3 ξ_c [29], where $\lambda_c=c/(0.65-0.5)$=20 Å, the maximum wave length of well defined excitations above magnetic transition temperature. This value ξ_c is accidentally close to the structural correlation length.

The inverse correlation length of critical fluctuations along the c direction is shown in Fig. 12 as a function of temperature obtained by Pouget *et al.* [16]. Solid curve is the best fit to the x-ray scattering data by a square root law. Our data obtained from neutron scattering are shown by open circles. Both anisotropy ratios of the structural and magnetic correration lengths agree near T_{SP}, but the magnetic correlation length along the c-direction at 15.3 K deviates from a square root law. Katoh and Imada [23] predict not to be divergent at T_{SP}. The magnetic correlation lengths may have a different behavior from the normal AF transition at T_{SP}. To clarify the relation of magnetic and structural correlations,

24
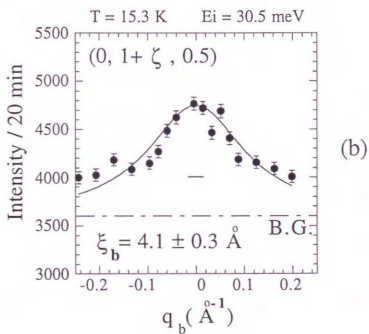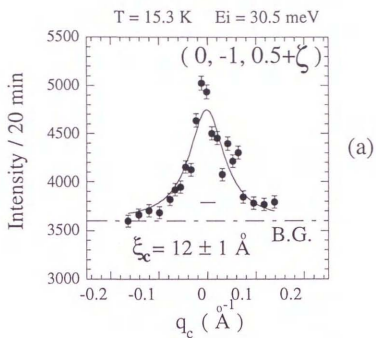
Fig. 10 (a)   Neutron critical scattering at 15.3K obtained by step scan along c^*-direction is shown. Horizontal bar indicates the resolution width.   (b) Step scan along b^*-direction with the same conditions as in (a). Solid line is a result fitted by Lorentzian.
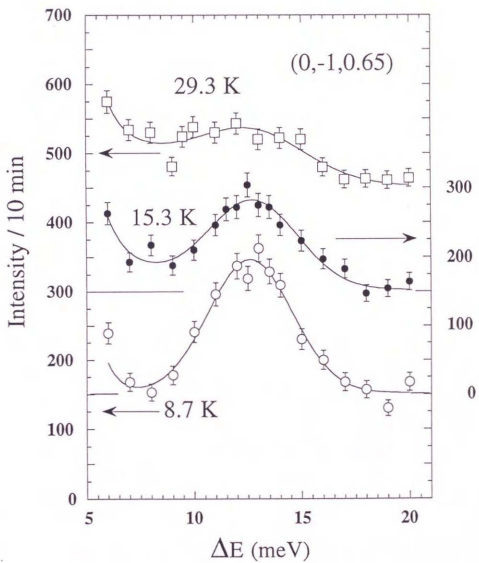
Fig. 11. Energy scan profiles of the magnetic excitations at (0,-1,0.65) in three different temperatures.
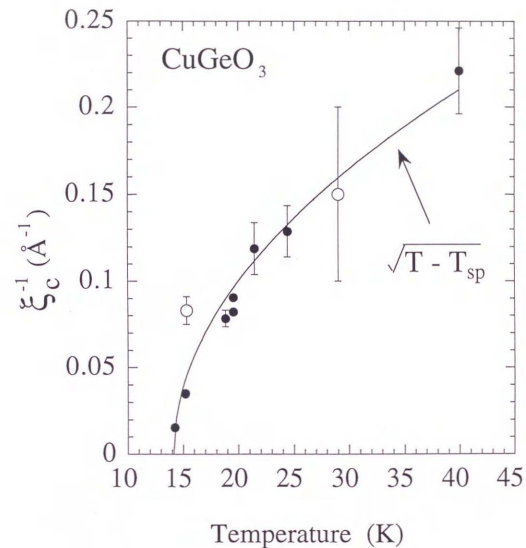
Fig. 12. Temperature dependence of inverse correlation length. Closed circles are the results from x-ray measurements by Pouget *et al.* [16]. Open circles from neutron scatterings by Nishi *et al.* [27]. Solid line shows the best fit of x-ray's data to the square root function of temperature.

more data upper and lower T_{SP} will be required. Lorenzo *et al.* [18] reported a remarkable soft longitudinal acoustic phonon along the *b*-axis. This results also indicates that $CuGeO_3$ has a low dimensional character crystallographically. If the inter chain coupling is weak, the Cu atom dimerization may arise.

3-2. Magnetic Field Dependence

Theoretically, the nature of the ground state and the properties of the SP gap in low-lying excitations have been subjects of interest [26]. The effect of a magnetic field on the SP transition has also been a subject for theoretical interests [30]. Experimentally, the phase diagrams in T and H space were determined in the organic SP systems and compared with the theoretical predictions [31]. However, no direct observation of SP gap as a function of magnetic field by inelastic neutron scattering was possible because the large single crystals of such organic substances were not available. In this chapter the results of an inelastic neutron scattering study of the magnetic excitation state was reported as a function of magnetic field up to 6 T [32,33].

(1) Horizontal Field (Unpolarized)

Performing the experiments in two different field configurations, (see Figure 13), the polarizations of the triplet modes observed under applied fields were determined. This is the first direct evidence for the theoretical result that the gap in a SP system corresponds to a singlet-triplet transition.

Inelastic neutron scattering experiment was performed using the unpolarized neutron with the fixed incident neutron energy, E_i=14.7 meV and the collimations, open(40')-20'-20'-40'. Horizontal field superconducting magnet (Oxford Instruments) capable of generating fields up to 6 T was used. The two pieces of single crystals with the sizes of 5ø×9 mm were mounted inside an aluminum can oriented so as to give crystallographic $(0, k, \ell)$ zones in the scattering plane. Because of the accessible scattering angle of the horizontal field superconducting magnet, only the excitations at reciprocal points
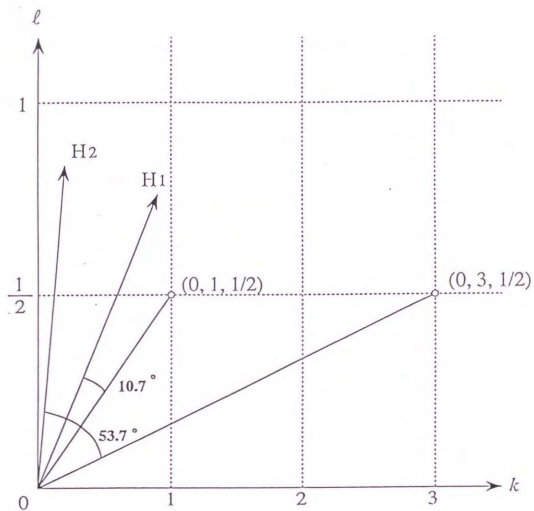
Fig. 13. The relationships between the scattering vectors and applied fields. The spectra at (0,1,1/2) and (0,3,1/2) were obtained at 5 K with field directions designated as the H_1 and H_2, respectively.

(0, 1, 1/2) and (0, 3, 1/2) were measured. Both reciprocal points are equivalent with smallest magnetic excitation gap (about 2 meV).

The relationships between the scattering vectors and the directions of the applied fields for these two configurations designated as H_1 and H_2 configuration, respectively, are depicted in Figure 13. These two configurations were chosen such that in H_1 the magnetic field direction is as parallel as possible to the scattering vector and in H_2 as perpendicular as possible to the scattering vector, at the same time allowing the energy scan up to about 3.7 meV energy transfer at these reciprocal points within the limited windows of the magnet. Therefore, the magnetic field direction H_1 was chosen as shown in Fig. 13 for the (0, 1, 1/2) reflection (H_1 configuration) and that of the H_2 for the (0, 3, 1/2) reflection (H_2 configuration), respectively. The angles between the magnetic field directions and the scattering vectors are $\alpha = 10.7$ deg. ($\sin^2(10.67°) = 0.034$) and 53.7 deg. ($\sin^2(53.7°) = 0.650$) for H_1 and H_2 configurations, respectively. Because of the selection rule for the magnetic neutron scattering, the cross section of the components of magnetic fluctuations can be seen in these configurations as

$$(1 + \cos^2\alpha) \cdot \langle M_\perp M_\perp \rangle + \sin^2\alpha \cdot \langle M_| M_| \rangle , \qquad (8)$$

where $\langle M_\perp M_\perp \rangle$ and $\langle M_| M_| \rangle$ denote magnetic fluctuations perpendicular and parallel to the applied magnetic field, respectively. Inserting the angles α,

$$(1 + 0.966) \langle M_\perp M_\perp \rangle + 0.034 \langle M_| M_| \rangle \qquad (9)$$

for H_1 configuration and

$$(1+0.350)\langle M_\perp M_\perp \rangle + 0.650\langle M_\parallel M_\parallel \rangle \qquad (10)$$

for H_2 configuration. The spectra in the H_1 configuration at $(0,1,1/2)$ under applied fields of 0, 1.5, 3.2, 4.5 and 6 T at 5 K are shown in Figure 14. The value of energy gap at zero field is 2.0 ± 0.1 meV, being in agreement with the previous data [14]. The splitting of this single gap at H=0 into upper and lower energies can be clearly observed.

Figure 15 shows the spectra in the H_2 configuration at $(0, 3, 1/2)$ under horizontal applied fields of 0 and 6 T at 5 K. The zero field result in this configuration shows a single peak at the same energy transfer as in H_1 configuration. In contrast to H_1 configuration, the development of a three peak structure under an applied field of 6 T is obvious.

In the H_1 configuration (Fig. 13), the scattering vector was almost parallel to the magnetic field ($\sin^2(10.67°)=0.034$), thereby only $\langle M_\perp M_\perp \rangle$ component was observed and $\langle M_\parallel M_\parallel \rangle$ component associated with the longitudinal spin fluctuation was not observed. On the other hand, in H_2 configuration (Fig. 15) we can see both the $\langle M_\parallel M_\parallel \rangle$ and $\langle M_\perp M_\perp \rangle$ components of the magnetic excitations at $(0, 3, 1/2)$. The appearance of a triplet peak structure under a magnetic field clearly demonstrates the spin excitation mode in three fold degenerate state. In order to know the accurate peak intensities and widths, we performed the Gaussian fitting procedure as expected from the instrumental resolution function. The small deviations of the line shapes at the wings at larger energy transfers cannot be attributed to the 'tailing' due to the resolution effect which stems from the steep slope of dispersion curve along c^*-direction, and should be related to SWDC as shown in Fig. 7(a).

Figure 16 depicts the field dependence of the energy positions of
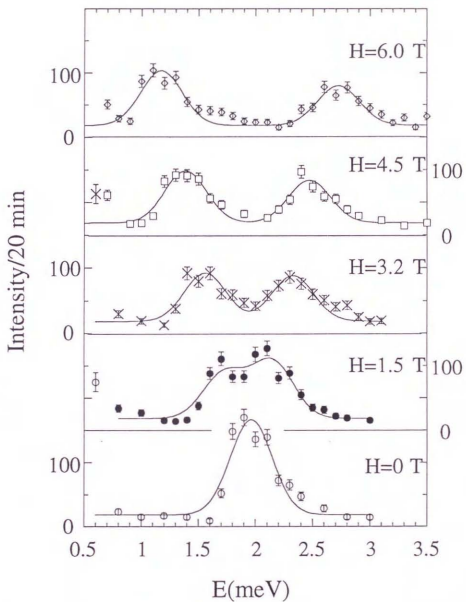
Fig. 14. The energy gaps at (0, 1, 1/2) at 5 K under the horizontal magnetic fields 0 T (open circle), 1.5 T (closed circle), 3.2 T (cross), 4.5 T (open square) and 6.0 T (open triangle), respectively.
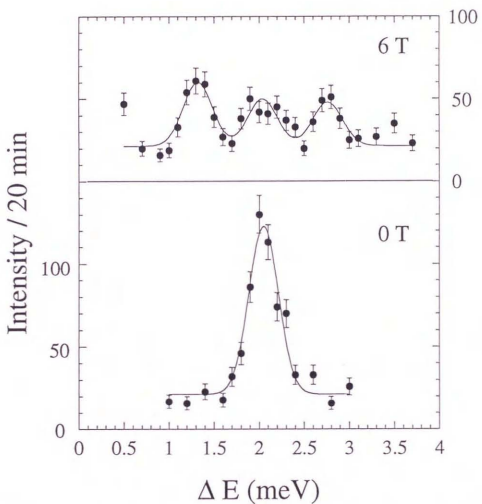
Fig. 15. The energy gap at (0, 3, 1/2) at 5 K under horizontal magnetic fields of 0 T and 6 T, respectively. Solid lines are the result fitted by a Gaussian function.
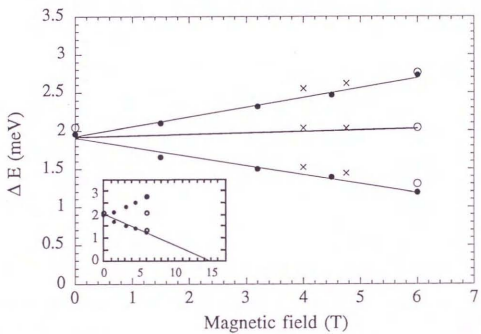
Fig. 16. Energy gap vs. horizontal magnetic fields at (0, 1, 1/2) (closed circles), (0, 3, 1/2) (open circles), and vertical magnetic field at (0, 1, 1/2) (crosses). Inset: Linear extrapolation of the lowest energy branch to $\Delta E=0$.

the observed gap energies as obtained from the Gaussian fits. It can be inferred that the field dependence of the energies is linear with a slope of ± 0.12 meV/T and that the energy splittings at (0, 1,1/2) and (0, 3, 1/2) are identical. This linear dependence can be well fitted by the equation $\Delta E = \Delta E(0) \pm g\mu_B H$, where g-values is 2.1. From the magnetization measurements [34], critical field H_c at which SP phase disappears and magnetic triplet phase appears is about 13 T. However, as shown in Fig. 4, the extrapolated value at $\Delta E = 0$ is 15 T. This discrepancy may be explained by the theoretical prediction that transition from the SP state to magnetic state may be the first order [35]. This should be confirmed under a higher magnetic field.

The fit results for the intensities of upper and lower energy peaks in Fig. 15 indicate that the intensities of these peaks in both configurations are equal, if one considers the known magnetic form factor for Cu^{2+} and the factor due to the magnetic selection rule as described above. This means that the intensities of $\langle M_\perp M_\perp \rangle$ observed in both configurations are same.

Comparing the intensities of $\langle M_\parallel M_\parallel \rangle$ and $\langle M_\perp M_\perp \rangle$ at (0, 3, 1/2) and 6 T, where both components are visible at the same time, it can be inferred from eq. (10) that the intensities associated to $\langle M_\parallel M_\parallel \rangle$ is identical with the intensities associated to $\langle M_\perp M_\perp \rangle$.

36

(2) Vertical Field (unpolarized)

An asymmetric superconducting magnet with a vertical field up to 4.75 T was used. The sample was oriented with its b^* and c^* axis in the scattering plane. Figure 17 shows a typical spectrum with the applied field of 4.75 T. The splitting of the single peak observed at 2 meV in zero field into a triple peak structure can be clearly seen. In Fig. 16 the energies observed in the vertical configuration at 4 and 4.75 T are marked with crosses together with the results of the horizontal field configuration with two different field directions in the b^*-c^* plane [32]. This result strongly suggests the isotropic nature of the gap mode because all three field directions yield the same field dependence of the Zeeman splitting modes.
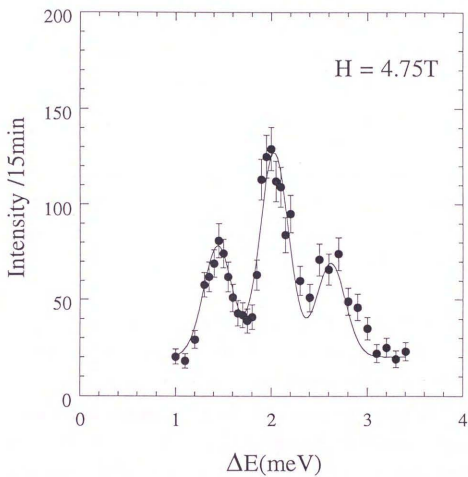
Fig. 17. Energy scan profile at (0, 1, 1/2) at 5 K under the vertical
magnetic field of 4.75 T.

(3)   Vertical Field (Polarized)

Polarized neutrons were employed in order to separate the $\langle M_{\parallel} M_{\parallel} \rangle$ and $\langle M_{\perp}M_{\perp} \rangle$ components unambiguously. When the polarization direction is perpendicular to the scattering vector, as it is the case here, the spin fluctuations parallel to the applied field are seen in the non-spin flip (NSF) process, and the spin fluctuations perpendicular to the applied field in the spin flip (SF) process [36]. The (1 1 1) reflection of magnetized Heusler alloy was used for monochromator and analyzer. The incident energy was fixed at 14.7 meV. Coarse horizontal collimations of open(40')-40'-40'-80' were used to partly compensate the intensity loss due to the polarization analysis. A DC flipper was introduced before the sample to obtain NSF scattering with flipper off state and SF scattering with flipper on state. A flipping ratio of about 20 was measured on a nuclear Bragg peak, yielding a neutron polarizing efficiency of about 90 %.

Figure 18 shows the results of the polarization analysis. NSF scattering is indicated by open points and SF scattering by closed points. Solid and broken lines are best fit with Gaussians. It is clear that the field independent peak and the two Zeeman split modes consist of $\langle M_{\parallel} M_{\parallel} \rangle$ and $\langle M_{\perp}M_{\perp} \rangle$, respectively. Considering these assignments of the fluctuations, the unpolarized neutron scattering results show that the intensities of $\langle M_{\parallel} M_{\parallel} \rangle$ and the sum of $\langle M_{\perp}M_{\perp} \rangle$ are equal in the vertical field configuration with the field of a^*-direction. Hence, it can be concluded that not only the energies, but also the detailed character of the spin fluctuations, i.e. the intensities of $\langle M_{\parallel} M_{\parallel} \rangle$ and $\langle M_{\perp}M_{\perp} \rangle$, do not depend on the field direction. All these results impressively demonstrate the isotropic nature of the gap mode.

This is consistent with the susceptibility measurements under

applied fields by Hase *et al.* [11], i.e. the Hamiltonian describing the magnetic system is very isotropic. Considering this isotropic nature, the splitting of the energy gap into three distinct levels under an applied field suggests that this is an exciton like transition from a non-magnetic singlet ground state to the magnetic triplet state in a SP system $CuGeO_3$.
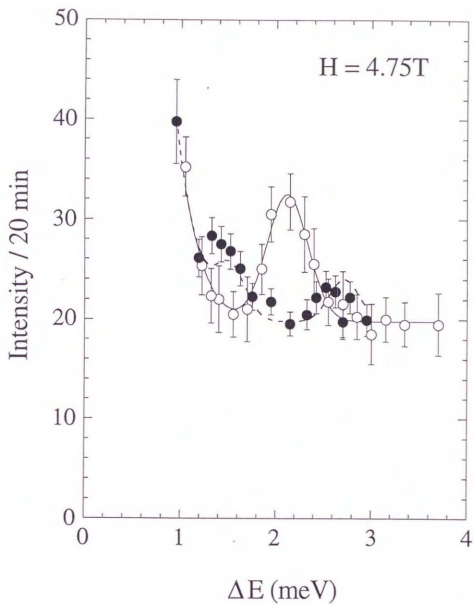
Fig. 18. Polarized neutron data at 4.3 K under the vertical magnetic field of 4.75 T. NSF and SF scattering are indicated by open and closed points, respectively.

3-3. Pressure Dependence

The organic SP systems were extensively studied, but an only few experiments were made under pressure. A variety of pressure dependence of T_{sp}'s are observed as tabulated in Table 2 [37,38,39,40]. One should note the difference of the sign of dT_{sp}/dP.

In 1991, Adams *et al.* [41] reported the pressure dependence of the lattice constants on $CuGeO_3$ using x-ray diffraction. All lattice constants decreased with increasing pressure up to 7 GPa at room temperature (RT). Recently, AC susceptibility and magnetic balance measurements have been performed on a single crystalline $CuGeO_3$ under high pressure up to 8 GPa and 1.1 GPa, respectively [40]. T_{sp} was increased linearly with increasing pressure at a rate of 4.8 K/GPa. The pressure dependence of the Curie constant C and Weiss temperature Θ were also obtained by fitting the susceptibility above T_{sp}.

To observe the pressure dependence of the SP gap, we tried the neutron inelastic scattering using a $CuGeO_3$ single crystal with the size 4 mmØ × 9 mm grown by traveling solvent floating zone method [42]. The incident neutron energy was fixed to be 13.7 meV and typical collimations were open(40')-40'-40'-80'. The SP gap was measured at $(0, 1, 1/2)$ in the $(0, k, \ell)$ scattering plane.

A clamping type high pressure cell used for neutron scattering at 5 K was mounted to the cold head of a closed cycle helium refrigerator. The single crystal $CuGeO_3$ was mounted with NaCl as a pressure standard in an Al micro-cell. Pressure was generated at RT using Fluorinert as the pressure-transmitting fluid and clamped by bolts and ring made from maraging steel [43]. The generated pressure was measured by monitoring the change of the lattice constant of single crystal NaCl.

The pressure dependence of the relative deviation of the lattice

Table 2. Spin-Peierls transition temperatures and their pressure
dependent coefficients observed until now. The data of $CuGeO_3$
were given by Takahashi *et al.* [40].

	T_{SP}	$\Delta T_{SP}/\Delta P$ (K/GPa)
TTF-CuBDT	11.5	-1.83 [37]
MEM-$(TCNQ)_2$	17.4	+18.6 [38]
$(TMTTTF)_2PF_6$	20	-6.57 [39]
$CuGeO_3$	14.1	+4.8 [40]

constants b and c at 5 K normalized by the RT values are shown in Fig. 19. Note that c-axis slightly elongates, while the b-axis remarkably shortens to 1.8 GPa. The temperature dependence of the three lattice constants was reported by BNL group [17,18,19] that the lattice constant c expanded with decreasing temperature and saturated below 20 K. A large contraction of the lattice constant b was also observed with decreasing temperature below T_{sp} in Ref. [18,19].

The spin excitation profiles observed at the (0,1,1/2) reflection by neutron inelastic scattering are shown in Fig. 20 at several pressures and at 5 K. Each pressure indicated in the figure was determined by the lattice constant of NaCl obtained from the (2 0 0) reflection. These peaks were fitted by a Gaussian function. A strong intensity rising at lower energy side stems from the strong incoherent background around $\Delta E=0$.

These SP gaps (Δ_{sp}) are plotted against pressure in Fig. 21, and Δ_{sp} is proportional to the pressure P; the ratio $\Delta_{sp}/P=1.3$ meV/GPa (15 K/GPa). The SP gap energy in high pressure cell at the atmospheric pressure (AP) is slightly different from the data on the same single crystal batch in the He gas atmosphere in the Al can. One possibility of this disagreement may come from the difference of thermal expansion coefficients between $CuGeO_3$ and Fluorinert.

To evaluate the intra-chain exchange parameter along the c-axis, we measured the dispersion relation at 1.8 GPa and at 4.3 K as shown in Fig. 22. The data at AP is also shown in the same figure. To observe the dispersion relation at high energy transfer was difficult because of the weak signals. Extrapolating the data to the zone boundary by the same method at AP, exchange constant J_c was roughly estimated to be 8.4±0.6 meV (100 K), that is about 0.8 times of the value at AP.

44
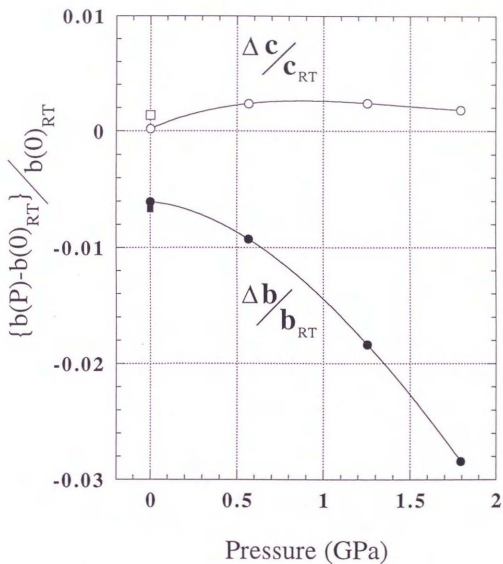
Fig. 19. The pressure dependence of the relative deviation of the
lattice constants, b and c at 5 K, normalized by b_{RT} and c_{RT}, $\{\Delta b/b_{RT}$
$= (b(P)-b_{RT})/b_{RT}\}$, where b_{RT} and c_{RT}, are the lattice constants at RT
and atmospheric pressure. Pressure was determined by the use of
(2 0 0) reflection of NaCl. Solid lines are guides to the eye.
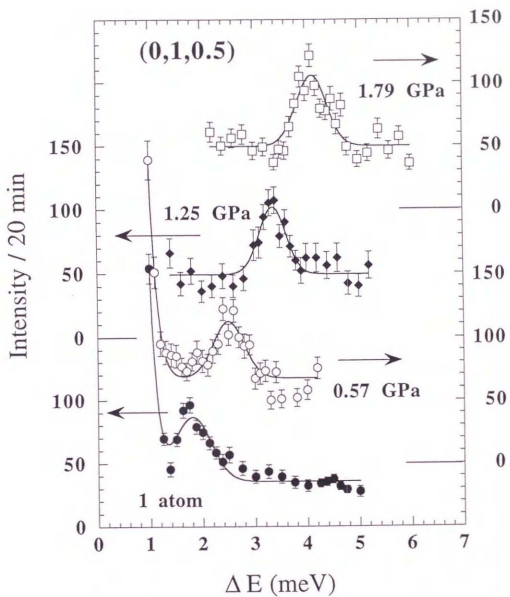
Fig. 20. Neutron scattering intensities of the (0, 1, 1/2) reflection measured at several pressures and at 5 K.

46
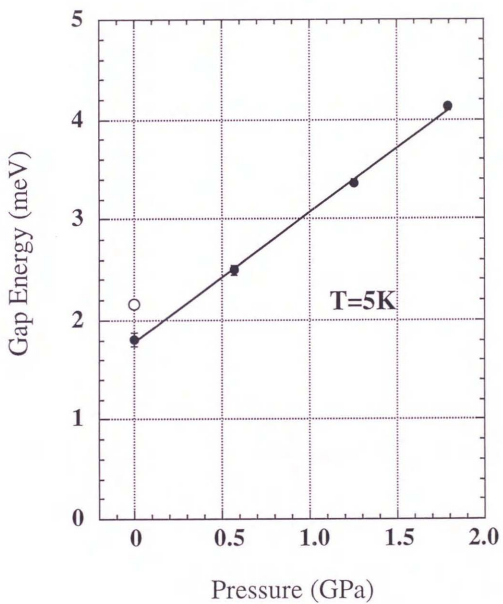
Fig. 21. Pressure dependence of the spin-Peierls gap at 5 K. Open circle shows the data at atmospheric pressure without the high pressure cell.
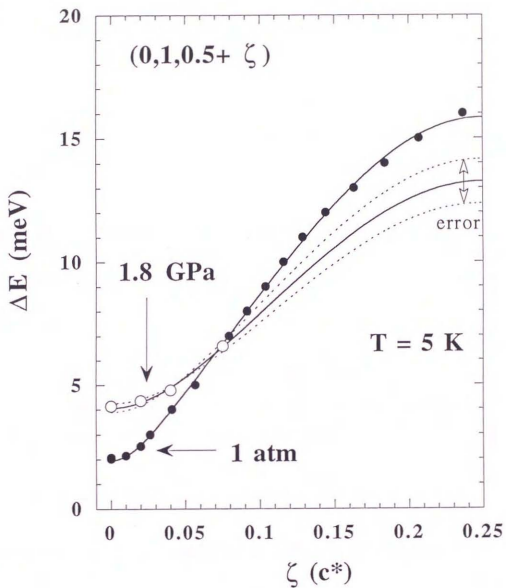
Fig. 22. The dispersion curve along the c^*-axis. Open circles and closed circles represent the data under 1.8 GPa and atmospheric pressure, respectively.

Chapter 4. Discussion

4-1. Spin Dynamics

(1) Dimerized State

In the SP system, one-dimensional spins couple to three-dimensional lattice distortions [8]; phenomena resembling with BCS theory in which conduction electrons make a singlet pair through the phonons. Therefore, to compare the SP energy gap to a superconductive one, we show the calculated values from the BCS equation, where the energy at 0 K is normalized to 2.1 meV. The temperature dependence of $CuGeO_3$'s SP energy gap does not agree with BCS equation and a much smaller critical exponent exists. These phenomena are caused by a one-dimensional quantum spin fluctuation in $CuGeO_3$. The equation $2\Delta(0) = 3.50\ T_{sp}$ is very close to the BCS formula $2\Delta(0) = 3.53\ T_{sp}$. The 2.1 meV (24.5 K) SP gap energy is in agreement with the value obtained by the magnetic susceptibility experiments [11]. When the lattice dimerizes, two unequal and alternating $J's$ are produced,

$$J_{1,2} = J_c \{1 \pm \delta(T)\}. \qquad (11)$$

Established result from the mean field theory gives as follows [6]

$$\delta(T) = \Delta(T)/pJ_c, \qquad (12)$$

where $p = 1 + 2/\pi$ at $T \ll J_c$.

Substituting $\Delta(0) = 24.5$ K and $J_c = 120$ K, we get $\delta(0) = 0.12$ and $J_2(0)/J_1(0) = 0.78$.

As can be seen in the spectra of constant Q scan (Figs. 7. (a) and (b)), the asymmetry in the line shape of magnetic excitation along

c^* is quite pronounced. In the constant energy scans in Fig. 8, similar discrepancy to a Gaussian profile was observed. These asymmetrical line shapes resemble with the first experimental observation of SWDC (spin-wave double continuum) in the uniform, $S=1/2$ Heisenberg AF chain, CPC by Heilmann et al. [3]. Exact quantum mechanical calculation of a finite, $S=1/2$ chain by Müller et al. [25] demonstrated the existence of an excitation continuum (SWDC) between lower and upper energy boundary given by eqs. (3) and (4). The lower energy boundary given by eq. (3) is the quantum renormalized spin wave dispersion relation given by des Cloizeaux and Pearson [2]. This is the first experimental evidence that the SWDC survives the dimerization of SP transition. One could imagine that once excitonic fluctuations were created in the non-magnetic, dimerized singlet ground state, they can propagate in the same manner as in the magnetic uniform chain.

Next we discuss the magnetic field dependencies of the energy gap in SP system. We note here that an energy gap due to a single site anisotropy term of the Hamiltonian in a classically $S=1/2$ ordered AF system splits to a doublet state, namely to up and down spins under a magnetic field. On the other hand, it is expected that a singlet state split to triplet state in SP system. There is an another class of system which shows nearly the same field dependence of the gap mode, namely Haldane systems with $S=1$. In both typical Haldane systems, NENP [44] and $CsNiCl_3$ [45], $\langle M_\perp M_\perp \rangle$ fluctuations show Zeeman splitting with a slope of ~0.12 meV/T, while $\langle M_\parallel M_\parallel \rangle$ mode remains unchanged. According to one of the theoretical pictures of a Haldane $S=1$ system [46], the individual $S=1$ spins are subdivided into two fictitious $S=1/2$ spins and the two neighboring $S=1/2$ spins, then form a singlet pair (valence bond). Since there is no static dimerization involved in this picture, one

might consider a dynamical singlet formation in this case. The above observation of the field dependence of the gap mode in SP and Haldane systems, therefore, strongly supports the static singlet formation in SP systems on one hand and the dynamical singlet formation in $S=1$ Haldane system on the other. The recent ESR result under applied magnetic fields up to 14 T by Brill *et al.* [47] could be explained by the magnetic transition from a singlet to triplet state, in qualitative agreement with the result presented here.

The pressure dependence of Δ_{sp} is represented by the following linear equation,

$$\Delta_{sp}(0) = 1.8 + 1.3\, P \qquad [\text{meV}]. \tag{13}$$

By measuring T_{sp}, as a function of pressure, on the other hand, Takahashi *et al.* [40] obtained

$$T_{sp} = 14 + 4.8\, P \qquad [\text{K}]. \tag{14}$$

From the equations (13) and (14), we obtained $2\Delta_{sp} \approx 4.2\ kT_{sp}$ at 1.8 GPa, which does not satisfy the BCS relation ($2\Delta_{sp}=3.53 kT_{sp}$), being asserted the consistency at AP by Nishi *et al.* [14].

According to the mean field theory [48,49], the SP gap can be described as $\Delta_{sp} =2.4 J_c \exp(-0.48\,\omega_0^2 J_c/g^2)$ where g is the spin-phonon coupling parameter proportional to derivative of J_c, $\partial J_c/\partial z$. ω_0 is characteristic phonon frequency at $q=2k_F$. In this case, g should be constant, because c-axis dose not change against pressure. For increasing Δ_{sp}, ω_0 must be decreased because of the constant g value. However, the phonon softening related to SP transition has not been observed so far, although much effort has been paid for the phonon measurement [50].

Referring the numerical calculations for the Heisenberg antiferromagnetic chain by Bonner-Blöte [26], the ratio $\alpha=J_2/J_1$, where J_1 and J_2 are the alternating exchange constants and the dimerization parameter $\delta=(1-\alpha)/(1+\alpha)$ were also evaluated as $\alpha=0.9$ and $\delta=0.06$ at AP, and as $\alpha=0.6$ and $\delta=0.2$ at 1.8 GPa, respectively. These values are different from the mean field theory in eqs. (11) and (12), and are more reliable than the approximate theory.

As was shown in refs. [15, 16], the superlattice reflections due to the lattice distortions appear at $(h+1/2, k, \ell+1/2)$ not at $(h, k, \ell+1/2)$. However, we observed the divergent nature of the neutron scattering intensity and it exponentially drops at $(0,1,1/2)$ in this system, clearly indicating that this wave vector point is magnetically original. In addition, we observed the magnetic field dependence between the singlet ground state and triplet excited state in SP phase of $CuGeO_3$ [32,33], showing that $(0, k, \ell+1/2)$ with k odd is actually the energy minimum point of the singlet state. Therefore, we concluded that the magnetic condensation wave vector to a spin singlet state was not the same with the superlattice wave vector in $CuGeO_3$.

(2) Uniform State

The temperature dependence of the static susceptibilities above T_{sp} in an organic SP systems TTF-CuBDT [6] and MEM(TCNQ)$_2$ [7] agrees with a theoretical curve proposed by Bonner-Fisher [12]. It apparently shows that the development of magnetic short range order is insensitive to the structural critical fluctuations. On the other hand, the static susceptibility of CuGeO$_3$ exhibited different behavior from the above organic systems. Liu *et al.* [51] proposed the characteristic temperature T_F which corresponds to the temperature where the structural correlation length just becomes comparable to the nearest neighbor distance of the magnetic atoms. In CuGeO$_3$, T_F is estimated to be around 80 K from the extrapolated curve of x-ray scattering on structural critical fluctuations [16]. Therefore, it is possible that the magnetic susceptibility of CuGeO$_3$ deviates at least from Bonner-Fisher curve below 80K.

We measured the magnetic critical scattering and we obtained the magnetic excitation profiles at several q at 8 K, 15.3 K, and 29 K [27]. The magnetic correlation length at 29 K was experimentally in good agreement with the structural correlation length. However, the magnetic correlation length at 15.3 K did not coincide with the structural correlation length. It is naturally understood that the structural correlation length of SP system diverges at T_{sp} on one hand, and the magnetic correlation length does not show the divergent nature on the other [23]. More data will be needed for the relationship between the magnetic and structural correlation lengths to study the critical behavior of the SP system.

4-2. Coupling to the Lattice

In the Peierls system discovered so far, KCP[52] and TTF-TCNQ[53], the longitudinal acoustic (LA) phonon along the chain axis softens at $q=2k_f(k_f$; Fermi wave vector) because the electron energy decreases by the splitting of the conduction band due to the lattice distortion. In the case of $CuGeO_3$, therefore, we speculated for the SP transition that the LA phonon along the chain axis softens at reciprocal lattice points $(h, k, \ell +1/2)$ due to the Cu-Cu spin's singlet coupling. We made the inelastic neutron scattering experiment on this phonon branch of $CuGeO_3$ [50]. The scattered neutron energy was fixed at $E_f= 30.5$ meV or 14.7 meV and horizontal collimators were set at open(40')-40'-40'-80'. The plate-like single crystal with size $45 \times 10 \times 3$ mm^3 was oriented with the [1 0 0] direction vertical. This configuration allows the measurement of the $(0, k, l)$ zone in the reciprocal lattice space. The Al sample can filled with He gas was set at the cold stage of a closed-cycle He refrigerator which could be cooled down to 4 K.

Figure 23(a) shows the clear two peaks at $\zeta=0.25$ of $(0, 0, 2+\zeta)$ reciprocal point at $T=200$ K. The intensity of clear peak at lower energy side decreases with increasing ζ and finally disappears at zone boundary (ZB, $\zeta=0.5$). Another peak shifts toward the higher energy with increasing ζ, and its energy reaches 40 meV at ZB.

The imaginary part of dynamical susceptibility $\chi''(q, \Delta E)$ obtained from the corrected spectra are shown in Fig. 23(b). The two distinct peaks observed at $\zeta=0.25$ may originate from the coupling between the longitudinal acoustic (LA) and longitudinal optical (LO) phonons.

Instead of clear peaks, we observed the pronounced broadened phonon peaks at large ζ-values of $(0, k, 2+\zeta)$ between $\zeta=0.25$ and 0.5 along the [0 0 1] direction. It is noted that these broad peaks are
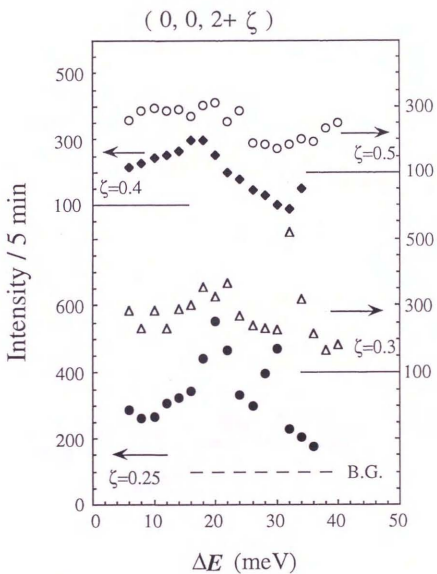
Fig. 23. (a) Phonon profiles of constant Q scan at 200 K with $E_f =$ 30.5 meV.
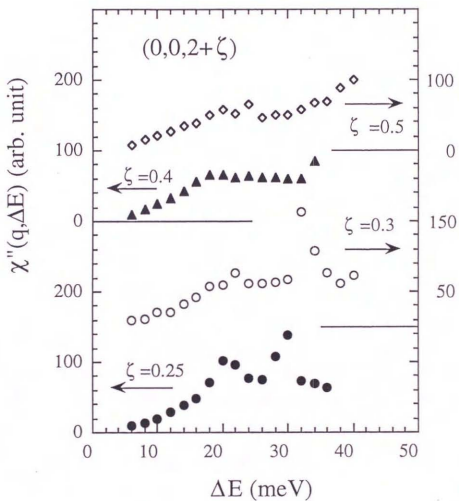
Fig. 23. (b) Imaginary part of dynamical susceptibility $\chi''(q, \Delta E)$ are obtained after subtracting the background and correcting the temperature factor from data (a).

observed almost independently of ζ between 0.25 and 0.5. The broad peaks at different ZB show the intrinsic broadness of this phonon profiles.

We obtained the another LO phonon profiles at $(0, 1, 2+\zeta)$ at T=14 K with E_f=30.5 meV (Fig. 24). We observed the same tendency to the $(0, 0, 2+\zeta)$, indicating that the peak intensity decreases and the width gradually broadens and its position shifts to higher energy side as increasing ζ. The [0 0 1] LO mode at $(0, 1, 2+\zeta)$ corresponds to the vibration with the inverse phase (the phase difference is just π) between two CuO_2 chains separated with a half of lattice constant b. The direction of this vibration is consistent to the Cu atom shifts observed in the superlattice reflections. It is reasonable that LO phonon width broadens due to the spin-phonon coupling in proportion as q closes to ZB. These phonon peaks may belong to the branch of the broad phonon peaks as shown in Fig. 23.

The dispersion curves of these branches were plotted against ζ in Fig. 25. We suggested that LO phonon in Fig. 24 would be linked to the broad phonon in Fig. 23, and that LO-phonon in Fig. 23 did not soften at ZB of $(0, 0, 2.5)$.

Lorenzo *et al.* showed the concave curve at near ζ=0.2 in [010] TA and LA phonon branches. They proposed the softening of LA mode, of which phonon energy is below TA mode, but Brillouin scattering data [54] did not show any anomaly from room temperature to 20 K in the [010] LA mode.

Now, proof of a strong spin-phonon coupling was obtained via phonon measurements using inelastic neutron scattering experiments [50]. These experiments showed that the phonon mode of $CuGeO_3$ becomes very broad at energies from 5 to 30 meV, hence indicating that the phonon couples to the magnetic excitation mode. Therefore, it is likely that the longitudinal acoustic phonon caused by the
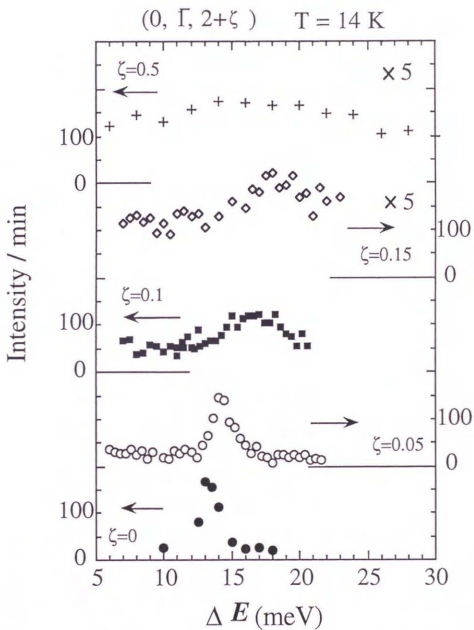
Fig. 24. Phonon profiles at $(0, 1, 2+\zeta)$ at 14 K with E_f= 30.5 meV.
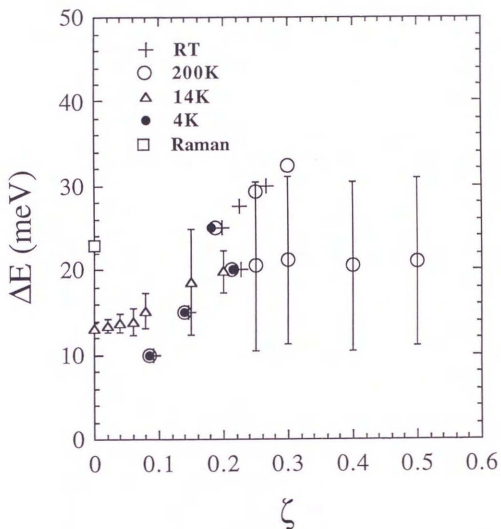
Fig. 25. The [0 0 1] LA phonon dispersion relations at $(0, k, 2+\zeta)$.
Raman data is shown with square [55].

Acoustic phonon couples to optical phonon at $\zeta = 0.2$. Temperature
dependence of the phonon is not remarkable. A vertical bar shows
the FWHM of LO branch at $(0, 1, 2+\zeta)$ and the broadened phonon
between $\zeta = 0.25$ and 0.5 .

dimerizing motion of the Cu-Cu atoms couples to the magnetic exciton.

In general the phonon width tends to broaden if it couples to another elementary excitation. We will report several experimental examples on broadened phonons coupled to another elementary excitation. Becoming a superconducting state below 18.3 K in Nb_3Sn [56], the spectral width of the phonon coupled to conduction electrons broadens as might have been expected from the BCS theory. In $Ni_{1-x}Pt_x$ alloys [57], since the localized mode of Pt atom coupled to acoustic phonon, the phonon profile of this resonance mode broadens. The crystal structure of TTF-CuBDT changes at about 240 K [58] and this crystal structure change plays an important role for the magnetic properties at low temperature. Broad phonon peaks in Figs. 23 and 24 might be related to the lattice instability or the intra-chain magnetic interaction of $CuGeO_3$. The origin of the broadness will be a future problem.

Chapter 5.   Summary and Conclusions

In this thesis work spin dynamics in the inorganic SP system $CuGeO_3$ has been extensively studied for the first time by means of neutron scattering. In a dimerized state a gap formation in the magnetic excitations was clearly observed as Δ_{sp}=2.1 meV at Q=(0, 1, 0.5). The dispersion relations along the three principal axes were determined. The correlation is strongest along the c-axis, giving J_c =10.4 meV while two inter chain exchanges are $J_b \approx 0.1 J_c$ and $J_a \approx$ -0.01J_c.

Under an applied magnetic field the direct evidence for the singlet-triplet transition in the dimerized state was obtained by inelastic neutron scattering. Applying magnetic field in the different field directions, the neutron intensities of $\left\langle M_\parallel M_\parallel \right\rangle$ and $\left\langle M_\perp M_\perp \right\rangle$ demonstrate the isotropic nature of the gap mode, hence supporting the excitonic description of the singlet-triplet transition at the AF zone center. The asymmetric line shape of the magnetic excitations at finite q suggests the existence of a SWDC above the lower triplet excitation boundary, and it is very similar to the uniform, S=1/2 AF chain.

Phonon measurements were also performed at several temperatures. A broad peak was observed at ΔE=21 meV with FWHM about 20 meV near the zone boundary along the [0 0 1] direction but it was almost independent of temperature.

The following interesting unsolved problems remain: (1) The soft phonon mode associated with the lattice dimerization has not been observed. (2) The role of the soft [010] LA mode in the SP transition is not clear. (3) Since the inter-chain exchange interaction is not so small, the antiferromagnetic order is expected to become more

stable than SP state. (4) The structure of M phase induced by a higher magnetic field still remains experimentally unsolved. (5) The pressure dependence of J_c, and T_{sp} or SP gap is inconsistent.

References

[1] H. A. Bethe, Z. Phys. **71** (1931) 205.

[2] J. des Cloizeaux and J. J. Pearson, Phys. Rev. **128** (1962) 2131.

[3] Y. Endoh, G. Shirane, R. J. Birgeneau, P. M. Richards and S. L. Holt, Phys. Rev. Lett. **32** (1974) 170; I. U. Heilmann, G. Shirane, Y. Endoh, R. J. Birgeneau, and S. L. Holt, Phys. Rev. **B18** (1978) 3530.

[4] S. E. Nagler, D. A. Tennant, R. A. Cowley, T. G. Perring, and S. K. Satija, Phys. Rev. **B44**, (1991) 12361.

[5] F. D. M. Haldane, Phys. Lett. **93A** (1983) 464; Phys. Rev. Lett. **50** (1983) 1153.

[6] J. W. Bray, H. R. Hart, L. V. Interrante, I. S. Jacobs, J. S. Kasper, G. D. Watkins, S. H. Wee, and J. C. Bonner, Phys. Rev. Lett. **35** (1975) 744.

[7] S. Huizinga, J. Kommandeur, G. A. Sawatzky, B. T. Thole, K. Kopinga, W. J. M. de Jonge, and J. Roos, Phys. Rev. **B 19** (1979) 4723.

[8] I. S. Jacobs, J. W. Bray, H. R. Hart, Jr. L. V. Interante, J. S. Kasper, G. D. Watkins, D. E. Prober, and J. C. Bonner, Phys. Rev. **B14** (1976) 3036.

[9] C. S. Jacobsen, H. J. Pedersen, Kell Mortensen, and K. Bechgaard, J. Phys. C: Solid State Phys., **13** (1980) 3411.

[10] C. F. Schwerdtfeger, S. Oostra, and G. A. Sawatzky, Phys. Rev. **B 25** (1982) 1786.

[11] M. Hase, I. Terasaki, and K. Uchinokura, Phys. Rev. Lett. **70** (1993) 3651.

[12] J. C. Bonner, and M. E. Fisher, Phys. Rev. **135** (1964) A640.

[13] M. Hase, I. Terasaki, K. Uchinokura, M. Tokunaga, N. Miura, and H. Obara, Phys. Rev. **B 48** (1993) 9616.

[14] M. Nishi, O. Fujita, and J. Akimitsu, Phys. Rev. **B50** (1994) 6508.

[15] O. Kamimura, M. Terauchi, M. Tanaka, O. Fujita, and J. Akimitsu, J. Phys. Soc. Jpn. **63** (1994) 2467.

[16] J. P. Pouget, L. P. Regnault, M. Aïn, B. Hennion, J. P. Renard, P. Veillet, G. Dhalenne, and A. Revcolevschi, Phys. Rev. Lett. **72** (1994) 4037.

[17] K. Hirota, D. E. Cox, J. E. Lorenzo, G. Shirane, J. M. Tranquada, M. Hase, K. Uchinokura, K. Kojima, Y. Shibuya, and I. Tanaka, Phys. Rev. Lett. **73** (1994) 736.

[18] J. E. Lorenzo, K. Hirota, G. Shirane, J. M. Tranquada, M. Hase, K. Uchinokura, H. Kojima, I. Tanaka, and Y. Shibuya, Phys. Rev. **B50** (1994) 1278.

[19] Q. J. Harris, Q. Feng, R. J. Birgeneau, K. Hirota, K. Kakurai, J. E. Lorenzo, G. Shirane, M. Hase, K. Uchinokura, H. Kojima, I. Tanaka, and Y. Shibuya, Phys. Rev. **B50** (1994) 12606.

[20] H. Völlenkle, A. Wittmann, and H. Nowotny, Monat. Chem. **98** (1967) 1352.

[21] S. Katano, H. Nakata, J. Akimitsu, F. Izumi, and M. Nishi, private communication.

[22] W Marshall and S. W. Lovesey, *Theory of Thermal Neutron Scattering*, (ed. Oxford at the Clarendon Press) (1971) 305.

[23] N. Katoh and M. Imada, J. Phys. Soc. Jpn. **63** (1994) 4529;
N. Katoh and M. Imada, J. Phys. Soc. Jpn. **62** (1993) 3728.

[24] M. T. Hutchings, H. Ikeda, and J. M. Milne, J. Phys. **C12** (1979) L739; S. K. Satija, J. D. Axe, G. Shirane, H. Yoshizawa, and K. Hirakawa, Phys. Rev. **B 21** (1980) 2001.

[25] G. Müller, H. Beck, and J. C. Bonner, Phys. Rev. Lett. **43** (1979) 75.

[26] J. C. Bonner and H. W. J. Blöte, Phys. Rev. **B25** (1982) 6959.

[27] M. Nishi, O. Fujita, J. Akimitsu, K. Kakurai, and Y. Fujii, to be published in Physica **B**.

[28] W. Marshall and R. D. Lowde, Rep. Prog. Phys. **31** (1968) 705.

[29] M. T. Hutchings, G. Shirane, R. J. Birgeneau, and S. L. Holt, Phys. Rev. **B5** (1972) 1999.

[30] M. C. Cross and D. S. Fisher, Phys. Rev. **B19** (1979) 402.

[31] D. Bloch, J. Voiron, J. C. Bonner, J. W. Bray, I. S. Jacobs, and L. V. Interrante, Phys. Rev. Lett. **44** (1980) 294.

[32] O. Fujita, J. Akimitsu, M. Nishi, and K. Kakurai, Phys. Rev. Lett. **74** (1995) 1677.

[33] O. Fujita, J. Akimitsu, M. Nishi, K. Kakurai, and Y. Fujii, to be published in Physica **B**.

[34] H. Ohta, S. Imagawa, Y. Yamamoto, M. Motokawa, O. Fujita, and J. Akimitsu, J. Phys. Soc. Jpn. **63** (1994) 2870.

[35] K. Hida, private communication.

[36] see e.g. K. Kakurai, M. Steiner and R. Pynn, Int. J. Mod. Phys. **7** (1993) 3095.

[37] J. W. Bray, L. V. Interrante, I. S. Jacobs, and J. C. Bonner, *Extended Linear Chain Compound*, 353-415, edited by J. S. Miller (1982) vol. 3.

[38] D. Bloch, J. Voiron, C. Vettier, J. W. Bray, and S. Oostra, Physica **119B** (1983) 43.

[39] L. G. Garon, F. Creuzet, P. Butaud, C. Bourbonais, D. Jérôme, and K. Bechgaard, Synthetic Metals **27** (1988) B123.

[40] H. Takahashi, N. Môri, O. Fujita, J. Akimitsu, and T. Matsumoto, to be published in Solid State Commun.

[41] D. N. Adams, J. Haines, and S. Leonard, J. Phys.: Condens Matter **3** (1991) 5183.

[42] M. Nishi, O. Fujita, J. Akimitsu, K. Kakurai, and Y. Fujii,

65

submitted to Phys. Rev. **B**.

[43] A. Onodera, Y. Nakai, N. Kunitomi, O.A. Pringle, H. G. Smith, R. M. Nicklow, R. M. Moon, F. Amita, N. Yamamoto, S. Kawano, N. Achiwa, and Y. Endoh, Jpn. J. Appl. Phys. **26** (1987) 152.

[44] L. P. Regnault, C. Vettier, J. Rossat-Mignod, and J. P. Renard, Physica **B 180 &181** (1992) 188.

[45] K. Kakurai, M. Steiner, R. Pynn, and J. K. Kjems, J. Phys: Condens. Matter **3** (1991) 715 .

[46] I. Affleck, T. Kennedy, E. H. Lieb, H. Tasaki, Phys. Rev. Lett. **59** (1987) 799.

[47] T. M. Brill, J. P. Boucher, J. Voiron, G. Dhalenne, A. Revcolevschi, and J. P. Renard, Phys. Rev. Lett. **73** (1994) 1545.

[48] J. W. Bray, Solid State Commun. **35** (1980) 853.

[49] Y. Lépine, Solid State Commun. **57** (1986) 189.

[50] M. Nishi, O. Fujita, J. Akimitsu, Physica **B210** (1995) 149.

[51] Q. Liu, S. Ravy, J. P. Pouget, C. Coulon, and C. Bourbonnais, Synthetic Metals **55-57** (1993) 1840.

[52] B. Renker, H. Rietsch, L. Pintschovius, W. Gläser, P. Brüesh, D. Kuse, and M. J. Rice, Phys. Rev. Lett. **30** (1973) 1144;

K. Carneiro, G. Shirane, S. A. Werner, and S. Kaiser, Phys. Rev. **B13** (1976) 4258.

[53] G. Shirane, S. M. Shapiro, R. Comés, A. F. Garito, and A. J. Heeger, Phys. Rev. **B14** (1976) 2325.

[54] H. Yamaguchi, M. Yamaguchi, and T. Yagi, to be published in J. Phys. Soc. Jpn.

[55] D. M. Adams and A. Fletcher, Spectrochimica Acta **44A** (1988) 233; M. Udagawa, H. Aoki, N. Ogita, O. Fujita, A. Sohma, A. Ogihara, and J. Akimitsu, J. Phys. Soc. Jpn. **63** (1994) 4060;

S. Sugai, J. Phys. Soc. Jpn. **62** (1993) 3829; H. Kuroe, T. Sekine, M. Hase, Y. Sasago, K. Uchinokura, H. Kojima, I. Tanaka, and Y.

Shibuya, Phys. Rev. B50 (1994) 16468.

[56] J. D. Axe and G. Shirane, Phys. Rev. Lett. **30** (1973) 214;
J. D. Axe and G. Shirane, Phys. Rev. **B8** (1973) 1965 .

[57] Y. Tsunoda, N. Kunitomi, N. Wakabayashi, R. M. Nicklow, and H. G. Smith, Phys. Rev. **B19** (1979) 2876.

[58] D. E. Moncton, R. J. Birgeneau, L. V. Interrante, and F. Wudl, Phys. Rev. Lett. **39** (1977) 507.